Title

Severe SARS-CoV-2 infection in humans is defined by a shift in the serum lipidome resulting in

dysregulation of eicosanoid immune mediators

Benjamin Schwarz[1&], Lokesh Sharma[2&], Lydia Roberts[1&], Xiaohua Peng[2], Santos Bermejo[2], Ian

Leighton[1], Arnau Casanovas Massana[3], Shelli Farhadian[4], Albert I. Ko[3], Yale IMPACT Team,

Charles S. Dela Cruz[2$*], Catharine M. Bosio[1$*]

[1]Laboratory of Bacteriology, National Institute of Allergy and Infectious Diseases, National Institutes of

Health, Hamilton, MT, USA [2]Section of Pulmonary and Critical Care and Sleep Medicine, Yale University

School of Medicine, New Haven, Connecticut [3]Department of Epidemiology of Microbial Diseases, Yale

School of Public Health, New Haven, CT 06520 [4]Department of Medicine, Section of Infectious Diseases,

Yale University School of Medicine, New Haven, CT, 06520

[&]Authors contributed equally

[$]Authors contributed equally

*Corresponding authors:

Catharine M Bosio: bosioc@niaid.nih.gov

Charles S. Dela Cruz: Charles.delacruz@yale.edu

Abbreviations

LM-eicosanoid and docosanoid lipid mediators, PE-phosphatidylethanolamine, LPE- lyso-PE, PC-

phosphatidylcholine, LPC-lyso-PC, PS-phosphatidylserine, PE(O) or PE(P)- plasmenyl or plasmanyl

plasmalogen, TAG- triacylglycerol, DAG-diacylglycerol, MAG-monoacylglycerol, CE-cholesterol ester, Cer-

ceramide, DCer- dihydroceramide, HCer-hexosylceramide, LCer-lactosylceramide, SM-sphingomyelin,

FAC-frees fatty acid, Rv-resolvin, LX-lipoxin, LT-luekotriene, HETE- hydroxyeicosatetraenoic acid, HEPE-

hydroxyeicosapentaenoic acid, HDHA- hydroxydocosahexaenoic acid, HDPA- hydroxydocosapentaenoic

acid, PG-prostaglandin, PD- D-series protectin, TxB2- Thromboxane B2, LC-MS/MS- liquid

chromatography tandem mass spectrometry, CBA- cytometric bead array, PCA- principle component

analysis, PLSDA- partial least square discriminant analysis

Introductory Paragraph

The COVID-19 pandemic has affected more than 10 million people worldwide with mortality exceeding half a million patients. Risk factors associated with severe disease and mortality include advanced age, hypertension, diabetes, and obesity.[1] Clear mechanistic understanding of how these comorbidities converge to enable severe infection is lacking. Notably each of these risk factors pathologically disrupts the lipidome and this disruption may be a unifying feature of severe COVID-19.[1-7] Here we provide the first in depth interrogation of lipidomic changes, including structural-lipids as well as the eicosanoids and docosanoids lipid mediators (LMs), that mark COVID-19 disease severity. Our data reveal that progression from moderate to severe disease is marked by a loss of specific immune regulatory LMs and increased pro-inflammatory species. Given the important immune regulatory role of LMs, these data provide mechanistic insight into the immune balance in COVID-19 and potential targets for therapy with currently approved pharmaceuticals.[8]

Main Text

Lipids function in disease to rearrange cellular signaling structures, modify metabolic processes, absorb reactive species, and act directly as both autocrine and endocrine ligands in the regulation of the immune system. Susceptibility to COVID-19 disease is strongly associated with pre-existing conditions characterized by dysregulation of the lipidome and metabolome.[4-6] While several studies have examined the systemic metabolic correlates of COVID-19, a well resolved interrogation of the lipidomic changes in COVID-19 severity has not been pursued.[9-12] To measure lipidomic changes in COVID-19 and gain mechanistic insights into how these changes may drive disease severity, we used serum draws from 19 healthy patients (healthy), 18 COVID-19 patients who did not require ICU admission (moderate) and 20 patients that required ICU admission (severe). The demographics, preexisting conditions, and treatment details of these patients are indicated in Table 1. Lipid and metabolite measurements were made using a series of targeted LC-MS/MS methods providing high-confidence feature identification.[13,14] Importantly for lipidomic analysis, this enabled the resolution of acyl-chain length and degree of unsaturation, which are both essential for understanding structural and functional rearrangement of the lipidome.

Changes in primarily polar metabolites among COVID-19 patient cohorts from China, Italy, and France have been reported.[9-12] In agreement with those studies, we observed a dysregulation of amino acid pools, interruption of the glucose to lactate balance, and dysregulation of nucleotide catabolic products such as xanthine, hypoxanthine, and urate (Sup. Fig. 1a-d).[9-12] These indicators suggest a robust xanthine oxidase stress response, associated with heart disease,[15-17] and likely reflect the degree of hypoxia/hypoxemia in the patient, which is a known to be associated with COVID-19 mortality.[18-22] These data also indicate broad agreement across international populations in metabolic correlates of COVID-19.

37   We next measured lipidomic profiles across severe and moderate COVID-19 infection along with the

38   healthy controls. To ensure comprehensive recovery of lipid classes, we utilized a modified chloroform

39   extraction method to recover both neutral and polar lipids.[23-25] By unbiased principle component

40   analysis (PCA), infected patients segregated from healthy in the negative ionization dataset but

41   overlapped in the positive ionization dataset (Sup. Fig. 2a-d). Group-biased partial least square

42   discriminant analysis (PLSDA) of the combined lipid dataset shows non-overlapping healthy and infected

43   separation across the primary axis of variance and a subgroup of severe patients that separate across

44   the secondary axis of variance (Fig. 1a). Specifically, the infected cohorts were associated with increased

45   levels of free poly-unsaturated fatty acids (PUFAs), rearrangement of certain sphingomyelins, and

46   decreased levels of PUFA-containing plasmalogens (Fig. 1b). Parallel univariate analysis revealed that

47   numerous neutral lipids significantly varied between severe and healthy controls, which may reflect

48   either changes in metabolism during infection or pre-infection differences in lipid levels due to pre-

49   existing conditions such as obesity (Sup. Fig 2e-g). Minor patterns distinguishing both infected from

50   healthy cohorts and moderate from severe disease were observed across lysophospholipids (Sup. Fig.

51   2h-j), cholesterol esters (chol-est) (Sup. Fig. 2k-m), and sphingolipids (Sup. Fig. 2n-p).

52   Across all lipid classes, PUFA containing lipids were abundant amongst the pool significantly varied lipids

53   between COVID-19 patients and healthy controls (Fig. 1c-e). To examine the regulation of PUFAs

54   between lipid classes and patient groups, we categorized lipids containing C20:4, C20:5, C22:5 or C22:6,

55   which likely represent arachidonic acid (AA), eicosapentaenoic acid (EPA), docosapentaenoic acid (DPA),

56   and docosahexaenoic acid (DHA). Of these PUFA-containing families, changes in the C20:4 series were

57   overrepresented in infected cohorts and could distinguish the severe from the moderate disease

58   patients (Fig. 1c-e). Many of these differentially regulated C20:4 species were the same plasmalogen

59   species that drove separation between infected and healthy cohorts by PCA (Sup. Fig. 2b) and PLSDA

60   (Fig. 2b, f-h). Interestingly, the depletion of PUFA-containing plasmalogen and increased levels of the

61   corresponding free-fatty acids (FAC) indicates the disease progression from the moderate to the severe

62   disease across each PUFA family (Fig. 1i-l). Plasmalogen is known to be a primary pool of PUFAs in both

63   immune and structural cells.[2,26] Upon systemic immune activation, PUFAs are liberated from their parent

64   glycerolipids and subsequently converted to a wide variety of immune signaling eicosanoids and

65   docosanoids.[27-32] The balance between pro-inflammatory, immune-regulating, and pro-resolving lipid

66   mediators can drastically change the efficacy of the immune response during infectious and sterile

67   inflammatory diseases as well as during the successful resolution of inflammation following disease.[33-35]

68   Therefore, we assessed the correlation of the eicosanoid and docosanoid species with COVID-19 disease

69   severity. We targeted 67 eicosanoid and docosanoid species using LC-MS/MS and 15 cytokines by

70   Cytometric Bead Array (CBA) or ELISA to relate lipid changes to markers of disease severity. Eicosanoid

71   and docosanoid lipid mediator (LM) signals were assessed by comparison to standards and available

72   spectral libraries (Sup. Fig. 3-5).[36] PCA analysis of the combined LM and cytokine data showed separation

73   of infected and healthy cohorts and overlapping, but distinct, separation between moderate and severe

74   patients (Fig. 2a). Nearly all LMs measured were positively correlated with infection (Fig. 2b). Univariate

75   analysis showed significant enrichment of the majority of LMs measured in both the moderate and

76   severe groups (Fig. 2c, d). Interestingly, moderate and severe disease were characterized by unique

77   milieus of LMs and cytokines (Fig. 2b, e). Moderate disease was characterized by significantly higher

78   levels of the pro-resolving LM resolvin E3 (RvE3). Further, there was a trend toward increased presence

79   of the prostaglandin family members, particularly PGE2 (p= 0.105), PGFD2 (p= 0.220) and PGF2a (p=

80   0.242). In contrast, severe disease was characterized by a further increase in free PUFAs levels, AA-, EPA-

81   , DPA and DHA-derived mono-hydroxylated species and AA-derived dihydroxylated species (Fig. 2c-e).

82   This shift in specific immune regulatory LMs in severe disease suggests that an imbalance of LMs may

83   contribute to disease progression. LMs are generated by a single or a series of oxygenase mediated

84   conversions of the parent PUFA. To examine the potential contribution of each oxygenase enzyme to

85   the severe disease phenotype we grouped LMs according to synthesis pathway (Fig. 2g-k). Several LMs

86   are shared between multiple enzyme groups as they require sequential stereospecific hydroxylations.

87   This grouping revealed that moderate disease was characterized by higher cyclooxygenase activity (COX)

88   as well as certain products of ALOX12 while severe disease is characterized by greater activity of ALOX5

89   and cytochrome p450 (CYP) enzymes. This is good agreement with previous observations from

90   influenza, which associated symptom severity with ALOX5 activity.[37]

91   COVID-19 comorbidities including obesity, age, heart disease, and diabetes are characterized by

92   dysregulation of the homeostatic lipidome.[1,3] To assess the correlation of these conditions with the

93   shifts in LM pools and their glycerolipid precursors, we overlaid age, sex, BMI, diabetes, heart disease,

94   survival, and antiviral treatment onto the separate PCAs (Sup. Fig. 7-15). Age and sex were evenly

95   distributed across the infected cohort on all PCAs (Sup. Fig. 7, 8). Of the treatments examined, only

96   remdesivir showed a negative correlation with the disease severity (Sup. Fig. 9-11). BMI, diabetes, heart

97   disease and morbidity segregated with the severity of disease across all datasets (Sup. Fig. 12-15). From

98   this study, it is likely that the lipidomic imbalance associated with severe disease is at least partially a

99   consequence of homeostatic disruption of the lipidome due to these pre-existing conditions. It is likely

100   that these pre-existing lipidomic imbalances are further exacerbated during COVID-19 through

101   dysregulation of the LM response resulting in severe disease, impaired resolution and persistent

102   inflammation.

103   Elevation of ALOX5- and CYP-dependent LMs in severe COVID-19 patient sera suggested systemic

104   upregulation of these pathways. To examine the cellular origin of these enzymes in COVID-19 patients,

105   we interrogated a published single cell RNAseq dataset of COVID-19 patient PBMCs for expression of

106   ALOX and CYP genes (Sup. Fig. 6a, b).[38] *ALOX5* expression was detected in most of the 20 cell types

107   identified (Fig. 3a-b) with the highest expression in CD14 monocytes, CD16 monocytes, neutrophils, B

108   cells, and DCs (Fig. 3c). *ALOX5* expression was significantly increased in neutrophils and trended upward

7

109   in CD14 monocytes, CD16 monocytes, and developing neutrophils (a population found almost

110   exclusively in diseased individuals) from COVID-19 patients compared to healthy controls. Interestingly,

111   severe COVID-19 is characterized by elevated *ALOX5* expressing monocyte/macrophage population and

112   depletion of lymphocyte populations.[38-40] The absence of CYP genes in the blood was consistent with

113   the primarily hepatic localization of these enzymes.[41] These data suggest a systemic dysregulation of

114   ALOX5 and further support the metabolic dysregulation of the liver in severe disease.[42]

115

116 **Conclusion**

117 These results provide the first detailed lipidomic understanding of COVID-19 disease progression and

118 represent one of the first combinations of bulk lipidomic and eicosanoid data to map mobilization of

119 lipids in human infectious disease.[7,37] We provide evidence that a systemic lipid network consisting of

120 liberated PUFAs from plasmalogen and their subsequent conversion to LMs, capable of modulating

121 inflammatory responses, characterizes both the onset and severity of COVID-19. Specifically, the loss of

122 the immune regulatory prostaglandins and the increased production of AA-derived products of ALOX5

123 and cytochrome P450 provides both a measure of disease severity and a mechanistic understanding of

124 the immune balance allowing for patient recovery. [43] Importantly, these pathways are directly

125 targetable with drugs previously approved for use in other inflammatory conditions and, thus, provide

126 therapeutic opportunities to control severe COVID-19.[27,31]

127

9

Author Contributions

B.S., L.S., C.D.C and C.M.B. conceived of experiment. L.S., X.P., S.B., A.C.M, S. F. and A.I.K and the Yale

IMPACT Team enrolled patients and collected samples. B.S., L.R. and I.L. extracted samples and collected

data. B.S. conducted metabolomics and lipidomics analysis. L.R. conducted single cell RNAseq analysis

and cytokine analysis. B.S., L.R., L.S., C.D.C. and C.M.B wrote the manuscript. Yale Impact team: (Listed in

alphabetical order) Kelly Anastasio, Michael H. Askenase, Maria Batsu, , Sean Bickerton, Kristina Brower,

Molly L. Bucklin, Staci Cahill, , Yiyun Cao, Edward Courchaine, , Giuseppe DeIuliis, John Fournier, Bertie

Geng, Laura Glick, Akiko Iwasaki, Nathan Grubaugh, Chaney Kalinich, William Khoury-Hanold, Daniel

Kim, Lynda Knaggs, Maxine Kuang, Eriko Kudo, Joseph Lim, Melissa Linehan, Alice Lu-Culligan, , Anjelica

Martin, Irene Matos, David McDonald, Maksym Minasyan, M. Catherine Muenker, Nida Naushad, Allison

Nelson, Jessica Nouws, , Abeer Obaid, Camilla Odio, Saad Omer, Isabel Ott, Annsea Park, Hong-Jai Park,

10

152   Mary Petrone, Sarah Prophet, Harold Rahming, Tyler Rice, Kadi-Ann Rose, Lorenzo Sewanan, Denise

153   Shepard, Erin Silva, Michael Simonov, Mikhail Smolgovsky, , Nicole Sonnert, Yvette Strong, Codruta

154   Todeasa, Jordan Valdez, Sofia Velazquez, Pavithra Vijayakumar, Annie Watkins, Elizabeth B. White, Yexin

155   Yang

156   **Competing Interests**

157   The authors declare no competing interests

158

Materials and Methods

Ethics Statement

161   This study was approved by Yale Human Research Protection Program Institutional Review Boards

162   (FWA00002571, Protocol ID. 2000027690). Informed consents were obtained from all enrolled patients.

163   The healthy blood samples were obtained under the protocol (HIC 0901004619) before the onset of

164   COVID-19 outbreak.

Chemicals

166   Tributylamine was purchased from Millipore Sigma. LCMS grade water, methanol, isopropanol,

167   chloroform and acetic acid were purchased through Fisher Scientific. All lipid mediator standards were

168   purchased from Cayman Chemical.

Kits and Reagents

170   CBA kits were purchased from BD Biosciences.

Patient cohort and serum collection

172   Patients were recruited among those who were admitted to the Yale-New Haven Hospital between

173   March 18th and May 9th, 2020 and were positive for SARS-CoV-2 by RT-PCR from nasopharyngeal

174   and/or oropharyngeal swabs. Patients in this study were enrolled through the IMPACT biorepository

175   study after obtaining informed consent. Basic demographics and clinical information of study

176   participants were obtained and shown in Table 1.

177   Prior to thawing, all samples were gamma-irradiated (2 MRad) to inactivate potential infectious virus.

Sample processing for aqueous, organic, and lipid mediator extraction

179   For all LCMS methods LCMS grade solvents were used. Sample order was randomized throughout each

180   extraction. For aqueous and organic metabolites, 50 µL patient serum was aliquoted directly into 400 µL

181   of ice-cold methanol and 500 µL of ice-cold chloroform was added. Samples were agitated by shaking for

182 20 minutes at 4 °C and subsequently centrifuged at 16k xg for 20 minutes at 4 °C to induce layering. The

183 top (aqueous) layer and bottom (organic layer) were collected. The aqueous layer was diluted 1:10 in

184 50% methanol in water and prepared for LCMS injection. The organic layer was taken to dryness in a

185 Savant™ DNA120 SpeedVac™ concentrator (Thermo Fisher) and stored at -80 °C until analysis. At time of

186 analysis, samples were resuspended in 500 µL of 5 µg/mL butylated hydroxytoluene in 6:1

187 isopropanol:methanol and further diluted 1:3 in the same solvent combination for LC-M/MS injection.

188 **Lipid mediators sample processing and extraction**

189 Lipid mediators were extracted from patient serum as previously described.[44] Briefly 100 µL of serum

190 was aliquoted on ice and 1 ng each of d8-5-HETE, d5-RvD2, d5-LXA4, d4-LTB4, d4-PGE2 was added to

191 each sample followed by 400 µL of ice-cold methanol. Samples were incubated for 30 min at -20 °C to

192 allow precipitation of protein. Samples were centrifuged at 10k xg for 10 minutes and the supernatant

193 was collected in a fresh tube.

194 Solid phase extraction columns (Sep-Pak® 3 mL, 200 mg, C18, Waters Corporation) were conditioned in

195 vacuum manifold with 10 mL of methanol followed by 10 mL of water. One at a time to each

196 supernatant, 9 mL of acidified water (pH 3.5 with hydrochloric acid) was added and the samples was

197 quickly loaded onto column. The column was then washed to with 10 mL of water. Once samples were

198 loaded, columns were washed with 4 mL of hexanes and then lipid mediators were eluted with 8 mL of

199 methyl-formate. Samples were dried under nitrogen and resuspended in 100 µL of 1:1 water:methanol.

200 For LC-MS analysis 30 µL of each sample was injected.

201 **LC-MS/MS analysis**

202 Aqueous metabolite, lipid, and lipid mediator samples were analyzed using a series of targeted multiple-

203 reaction monitoring (MRM) methods. All samples were separated using a Sciex ExionLC™ AC system and

204 analyzed using a Sciex 5500 QTRAP® mass spectrometer.

205   Aqueous metabolites were analyzed using a previously established ion pairing method with

206   modification.[14] Quality control samples were injected after every 10 injections and assessed for signal

207   stability. Samples were separated across a Waters Atlantis T3 column (100Å, 3 µm, 3 mm X 100 mm) and

208   eluted using a binary gradient from 5 mM tributylamine, 5 mM acetic acid in 2% isopropanol, 5%

209   methanol, 93% water (v/v) to 100% isopropanol over 15 minutes. Analytes were detected in negative

210   mode using two distinct MRM pairs for each metabolite when possible. After signal confirmation only

211   one of the MRM signals was taken forward for analysis. Heavy labeled standards were not utilized given

212   the breadth of targets, thus relative quantification was performed. Fidelity of select signals including

213   retention time and spectra was confirmed by comparison to a synthetic molecular reference.

214   Lipid samples were analyzed using a previously established HILIC method with modification.[13] Samples

215   were separated on a Water XBridge® Amide column (3.5 µm, 3 mm X 100 mm) and eluted using a 12

216   minute binary gradient from 100% 5 mM ammonium acetate, 5% water in acetonitrile apparent pH 8.4

217   to 95% 5 mM ammonium acetate, 50% water in acetonitrile apparent pH 8.0. Target lipids were

218   detected using scheduled MRM. Lipid signals were divided into two methods utilizing either negative

219   mode or positive mode and a separate injection was analyzed for each method. Both datasets were

220   separately normalized using total-area sum to correct for instrument drift.

221   Lipid mediators were analyzed using a previously established reverse phase method with

222   modifications.[44] Samples were separated on a Waters Atlantis T3 column (100Å, 3 µm, 3 mm X 100 mm)

223   and using a binary gradient of A: 0.01 % acetic acid in water and B: 0.01 % acetic acid in methanol.

224   Samples were eluted over 20 min from 40-100 % B. Samples were detected in negative mode using

225   previously published MRM pairs and source conditions.[36] Triggered spectra were collected using

226   enhanced-product ion scans and rolling collision energy. A blank and a standard mix were serially

227   injected every 10 injections. Standard mix consisted of each of the following compounds at 10 ng/mL:

228   RvE3, LXA4, LXA5, LXB4, PGE2, PGD2, PGF2a, TxB2, PD1, RvD5, Maresin 1, LTB4, 5,15-DiHETE, 14-HDHA,

14

229   18-HEPE, AA, EPA, DHA. Spectra and comparison to authentic standards was used to confirm signal

230   identity.

231   Spectral confirmation was not possible for RvD2, RvD3, LXA5, RvD6, 8,9 DiHETrE, 12-HHT, 11-HETE, 11-

232   HEPE, 7-HDPA, 13-HDPA, 14-HDPA, 17-HDPA, 7-HDHA, 13-HDHA, 17-HDHA and 21-HDHA but identity

233   was assessed by comparison to related standards. These signals were regarded as lower confidence but

234   were used for class comparison of the LMs and multivariate analysis.

235   All signals were integrated using MultiQuant® Software 3.0.3. In total 1,414 molecules were targeted

236   across a water-soluble metabolite method and two organic-extracted lipid methods in either positive or

237   negative ionization modes. Of these 716 features were judged to be positively detected by visual

238   inspection, missing value filtering (50% cut-off) and QC coefficient of variance filtering (40% cut-off after

239   normalization). Remaining missing values were replaced with the minimum group value for that feature.

240   For aqueous and lipid mediator datasets signal quality was judged visually and signal stability was

241   assessed by QC or repeat injection of a standard mix. Lipid mediator data was normalized to internal

242   heavy isotope standards as previously described.[44]

243   Univariate and multivariate analysis was performed in MarkerView® Software 1.3.1. The aqueous

244   dataset and the combined lipid mediators/cytokine dataset data were autoscaled prior to multivariate

245   analysis in order to visualize the contribution of low ionization efficiency species and difference of scales

246   between the cytokine and lipid mediator measurements. Lipid datasets were pareto scaled to avoid

247   overrepresenting low abundance signals within each lipid class. For all univariate analysis an unpaired t-

248   test was used. For univariate analysis of the LM/cytokine set a single moderate group patient was

249   excluded by an extreme studentized deviate test for analysis of PGE2 (z = 4.58).

250   **Quantification of cytokine and chemokine levels**

251   The serum concentration of IFN-α, IFN-γ, IL-1β, IL-2, IL-4, IL-6, IL-8, IL-10, IL-12/IL-23p40, IL-17A, MIP-1α,

252   RANTES, TNF-α, and MCP-1 was determined using a cytometric bead array according to the

15

253   manufacturer's instructions (BD Biosciences). The serum concentration of IL-1α was determined by an

254   ELISA according to the manufacturer's instructions (R & D Systems).

255   **Single cell RNA sequencing analysis**

256   The published single cell RNA sequencing dataset from Wilk, et al Nature Medicine 2020 was

257   downloaded from the COVID-19 Cell Atlas (https://www.covid19cellatlas.org/#wilk20).[38] Data was read

258   into Seurat v3.0 and each cluster's cellular identity was annotated per Wilk, et al Nature Medicine

259   2020.[38] Expression levels of ALOX and CYP genes within specific cell types in healthy controls and COVID-

260   19 patients was visualized using Seurat's DotPlot feature. *ALOX5* expression levels in specific cell types

261   was visualized using the VlnPlot feature A Mann-Whitney test was used to determine statistical

262   differences in gene expression between healthy and COVID samples.

263   **Patient Statistics**

264   Demographic data is presented as either counts and percentages (for categorical data) or means and

265   standard deviations (for continuous data). To investigate the difference in the control, moderate and

266   severe groups, GraphPad Prism (version 8.4.2) was used. The results were compared using the chi-

267   square test or Fisher's exact test for categorical variables and one-way analysis of variance (ANOVA) or

268   unpaired t test was used for continuous variables. A p-value of less than 0.05 was considered statistically

269   significant.

270

16

References

1. Richardson, S., *et al.* Presenting characteristics, comorbidities, and outcomes among 5700 patients hospitalized with COVID-19 in the New York City area. *Jama* (2020).

2. Braverman, N.E. & Moser, A.B. Functions of plasmalogen lipids in health and disease. *Biochimica et Biophysica Acta (BBA)-Molecular Basis of Disease* **1822**, 1442-1452 (2012).

3. Yang, J., *et al.* Prevalence of comorbidities in the novel Wuhan coronavirus (COVID-19) infection: a systematic review and meta-analysis. *International journal of infectious diseases* (2020).

4. Bellis, C., *et al.* Human plasma lipidome is pleiotropically associated with cardiovascular risk factors and death. *Circulation: Cardiovascular Genetics* **7**, 854-863 (2014).

5. Pietiläinen, K.H., *et al.* Association of lipidome remodeling in the adipocyte membrane with acquired obesity in humans. *PLoS Biol* **9**, e1000623 (2011).

6. Sharma, S., *et al.* Role of oxidized lipids in pulmonary arterial hypertension. *Pulmonary circulation* **6**, 261-273 (2016).

7. Titz, B., *et al.* Alterations in serum polyunsaturated fatty acids and eicosanoids in patients with mild to moderate chronic obstructive pulmonary disease (COPD). *International journal of molecular sciences* **17**, 1583 (2016).

8. Pettersen, D., Davidsson, Ö. & Whatling, C. Recent advances for FLAP inhibitors. *Bioorganic & Medicinal Chemistry Letters* **25**, 2607-2612 (2015).

9. Blasco, H., *et al.* The specific metabolome profiling of patients infected by SARS-COV-2 supports the key role of tryptophan-nicotinamide pathway and cytosine metabolism. (Research Square, 2020).

10. Shen, B., *et al.* Proteomic and metabolomic characterization of COVID-19 patient sera. *Cell* (2020).

294   11.   Troisi, J.*, et al.* Serum metabolomic profile of symptomatic and asymptomatic SARS-CoV-2

295   infected patients. (2020).

296   12.   Wu, D.*, et al.* Plasma Metabolomic and Lipidomic Alterations Associated with COVID-19.

297   *medRxiv* (2020).

298   13.   Mackenzie Pearson, S.K.K., Wu, S. & Baker, P.R. Achieve Broad Lipid Quantitation using a High-

299   Throughput Targeted Lipidomics Method.

300   14.   McCloskey, D., Gangoiti, J.A., Palsson, B.O. & Feist, A.M. A pH and solvent optimized reverse-

301   phase ion-paring-LC–MS/MS method that leverages multiple scan-types for targeted absolute

302   quantification of intracellular metabolites. *Metabolomics* **11**, 1338-1350 (2015).

303   15.   Dawson, J. & Walters, M. Uric acid and xanthine oxidase: future therapeutic targets in the

304   prevention of cardiovascular disease? *British journal of clinical pharmacology* **62**, 633-644

305   (2006).

306   16.   Hare, J.M. & Johnson, R.J. Uric acid predicts clinical outcomes in heart failure: insights regarding

307   the role of xanthine oxidase and uric acid in disease pathophysiology. (Am Heart Assoc, 2003).

308   17.   Papi, A.*, et al.* Role of xanthine oxidase activation and reduced glutathione depletion in

309   rhinovirus induction of inflammation in respiratory epithelial cells. *Journal of Biological*

310   *Chemistry* **283**, 28595-28606 (2008).

311   18.   Tobin, M.J., Laghi, F. & Jubran, A. Why COVID-19 Silent Hypoxemia is Baffling to Physicians.

312   *American Journal of Respiratory and Critical Care Medicine* (2020).

313   19.   Chen, X.-Q., Dong, J., Niu, C.-Y., Fan, J.-M. & Du, J.-Z. Effects of hypoxia on glucose, insulin,

314   glucagon, and modulation by corticotropin-releasing factor receptor type 1 in the rat.

315   *Endocrinology* **148**, 3271-3278 (2007).

316   20.   Newhouse, L.P.*, et al.* Three hours of intermittent hypoxia increases circulating glucose levels in

317   healthy adults. *Physiological reports* **5**, e13106 (2017).

318   21.   Oltmanns, K.M.*, et al.* Hypoxia causes glucose intolerance in humans. *American journal of*

319   *respiratory and critical care medicine* **169**, 1231-1237 (2004).

320   22.   Xie, J.*, et al.* Association between hypoxemia and mortality in patients with COVID-19. in *Mayo*

321   *Clinic Proceedings* (Elsevier, 2020).

322   23.   Reis, A.*, et al.* A comparison of five lipid extraction solvent systems for lipidomic studies of

323   human LDL. *Journal of lipid research* **54**, 1812-1824 (2013).

324   24.   Tyagi, R.K., Azrad, A., Degani, H. & Salomon, Y. Simultaneous extraction of cellular lipids and

325   water-soluble metabolites: evaluation by NMR spectroscopy. *Magnetic resonance in medicine*

326   **35**, 194-200 (1996).

327   25.   Lin, C.Y., Wu, H., Tjeerdema, R.S. & Viant, M.R. Evaluation of metabolite extraction strategies

328   from tissue samples using NMR metabolomics. *Metabolomics* **3**, 55-67 (2007).

329   26.   Lebrero, P.*, et al.* Cellular plasmalogen content does not influence arachidonic acid levels or

330   distribution in macrophages: A role for cytosolic phospholipase A2γ in phospholipid remodeling.

331   *Cells* **8**, 799 (2019).

332   27.   Dennis, E.A. & Norris, P.C. Eicosanoid storm in infection and inflammation. *Nature Reviews*

333   *Immunology* **15**, 511-523 (2015).

334   28.   Norris, P.C., Gosselin, D., Reichart, D., Glass, C.K. & Dennis, E.A. Phospholipase A2 regulates

335   eicosanoid class switching during inflammasome activation. *Proceedings of the National*

336   *Academy of Sciences* **111**, 12746-12751 (2014).

337   29.   Dennis, E.A., Cao, J., Hsu, Y.-H., Magrioti, V. & Kokotos, G. Phospholipase A2 enzymes: physical

338   structure, biological function, disease implication, chemical inhibition, and therapeutic

339   intervention. *Chemical reviews* **111**, 6130-6185 (2011).

340   30.   Lämmermann, T.*, et al.* Neutrophil swarms require LTB4 and integrins at sites of cell death in

341   vivo. *Nature* **498**, 371-375 (2013).

19

342   31.   Bitto, A.*, et al.* Flavocoxid, a dual inhibitor of COX-2 and 5-LOX of natural origin, attenuates the

343   inflammatory response and protects mice from sepsis. *Critical Care* **16**, R32 (2012).

344   32.   Dalli, J. & Serhan, C.N. Specific lipid mediator signatures of human phagocytes: microparticles

345   stimulate macrophage efferocytosis and pro-resolving mediators. *Blood* **120**, e60-e72 (2012).

346   33.   Kowal-Bielecka, O.*, et al.* Cyclooxygenase-and lipoxygenase-derived eicosanoids in

347   bronchoalveolar lavage fluid from patients with scleroderma lung disease: An imbalance

348   between proinflammatory and antiinflammatory lipid mediators. *Arthritis & Rheumatism* **52**,

349   3783-3791 (2005).

350   34.   Serhan, C.N. & Haeggstrom, J. Lipid mediators in acute inflammation and resolution:

351   Eicosanoids, PAF, resolvins, and protectins. *Fundamentals of Inflammation. CN Serhan, PA Ward,*

352   *DW Gilroy, and SS Ayoub, editors. Cambridge University Press, Cambridge*, 153-174 (2010).

353   35.   Serhan, C.N. & Savill, J. Resolution of inflammation: the beginning programs the end. *Nature*

354   *immunology* **6**, 1191-1197 (2005).

355   36.   Ian Riley, P.C.N., Kathy Luong, Charles Serhan. CET&RI Spectra Book & Physical Properties of

356   SPM and Eicosanoids 2019. (2019).

357   37.   Tam, V.C.*, et al.* Lipidomic profiling of influenza infection identifies mediators that induce and

358   resolve inflammation. *Cell* **154**, 213-227 (2013).

359   38.   Wilk, A.J.*, et al.* A single-cell atlas of the peripheral immune response in patients with severe

360   COVID-19. *Nature Medicine*, 1-7 (2020).

361   39.   Liao, M.*, et al.* Single-cell landscape of bronchoalveolar immune cells in patients with COVID-19.

362   *Nature medicine*, 1-3 (2020).

363   40.   Merad, M. & Martin, J.C. Pathological inflammation in patients with COVID-19: a key role for

364   monocytes and macrophages. *Nature Reviews Immunology*, 1-8 (2020).

365 41. Renaud, H.J., Cui, J.Y., Khan, M. & Klaassen, C.D. Tissue distribution and gender-divergent

366   expression of 78 cytochrome P450 mRNAs in mice. *Toxicological sciences* **124**, 261-277 (2011).

367 42. Huang, C.*, et al.* Clinical features of patients infected with 2019 novel coronavirus in Wuhan,

368   China. *The lancet* **395**, 497-506 (2020).

369 43. Kalinski, P. Regulation of immune responses by prostaglandin E2. *The Journal of Immunology*

370   **188**, 21-28 (2012).

371 44. English, J.T., Norris, P.C., Hodges, R.R., Dartt, D.A. & Serhan, C.N. Identification and profiling of

372   specialized pro-resolving mediators in human tears by lipid mediator metabolomics.

373   *Prostaglandins, Leukotrienes and Essential Fatty Acids* **117**, 17-27 (2017).
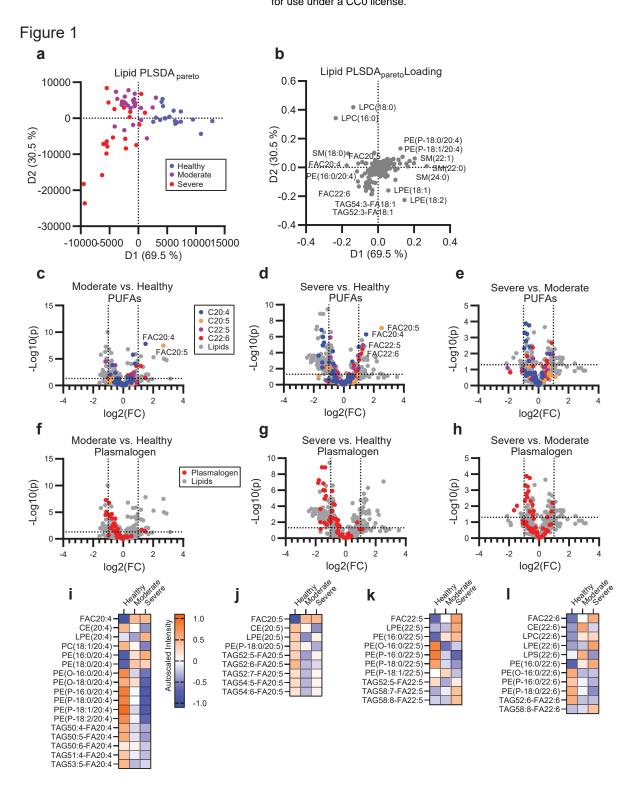
374

375

Figure Captions

Figure 1. Mobilization of plasmalogen-derived PUFAs correlates with the disease severity in COVID-19.

(a) Supervised PLSDA analysis of the healthy, moderate and severe disease groups and **(b)** the

corresponding feature loading plot. (c-e) Comparison of moderate to healthy **(c)**, severe to healthy **(d)**

and severe to moderate **(e)** by unpaired t-test with PUFA classes overlaid. Overlaid data series

correspond to lipid species containing at least one copy of C20:4 (blue), C20:5 (orange), C22:5 (purple)

or C22:6 (red) acyl chains. **(f-h)** Comparison of moderate to healthy **(f)**, severe to healthy **(g)** and severe

to moderate **(h)** by unpaired t-test with plasmalogen lipid series overlaid in red. For (c-h) cutoff lines

indicate a positive or negative 2-fold change and a p-value of 0.05. **(i-l)** Heatmap of the autoscaled mean

intensity of each patient group for significantly varied lipids (p<0.05) containing C20:4 **(i)**, C20:5 **(j)**, C22:5

(k), and C22:6 **(l)**. Color scale is consistent for (i-l).

Figure 2: A unique milieu of LMs defines moderate and severe COVID-19 disease. (a) Unsupervised PCA

of autoscaled combined lipid mediator and cytokine dataset and **(b)** corresponding feature loading plot.

(c-e) Univariate comparison of moderate disease to healthy **(c)**, severe disease to healthy **(d)** and severe

to moderate disease **(f)** by unpaired t-test. Cutoff lines indicate a positive or negative 2-fold change and

a p-value of 0.05. For (b-f) species are colored by class as cytokine (cyan), arachidonic acid-derived (AA-

derived, blue), eicosapentaenoic acid-derived (EPA-derived, orange), docosapentaenoic acid-derived

(DPA-derived, purple) or docosahexaenoic acid-derived (DHA-derived, red). **(f-k)** Heatmaps of the

autoscaled mean for each patient group across cytokines **(f)**, molecules synthesized by ALOX5 **(g)**,

ALOX12 **(h)**, ALOX15 **(i)**, Cyclooxygenases **(j)** or cytochrome P450 **(k)**. Color scale is consistent across (f-

k).

22

399   **Figure 3. Human PBMCs from COVID-19 patients are enriched for *ALOX5* expressing cells and express**

400   **higher levels of *ALOX5*. (a)** UMAP dimensionality reduction plot of a published human PBMC single-cell

401   RNA Seq dataset (Wilk, et al *Nature Medicine* 2020) identifying twenty cell types. **(b)** UMAP depicting

402   *ALOX5* expressing cells in blue. **(c)** Violin plots indicating *ALOX5* expression levels within specific cellular

403   populations in healthy (blue) or COVID (red) PBMCs. Statistical significance was determined by a Mann-

404   Whitney test; * $p < 0.05$. ** $p < 0.01$.

405

406

407 **Table 1. Patient demographics, preexisting conditions and treatment distributions.** Patient data were

408 compared using the chi-square test or Fisher's exact test for categorical variables and one-way analysis

409 of variance (ANOVA) or unpaired t test was used for continuous variables.

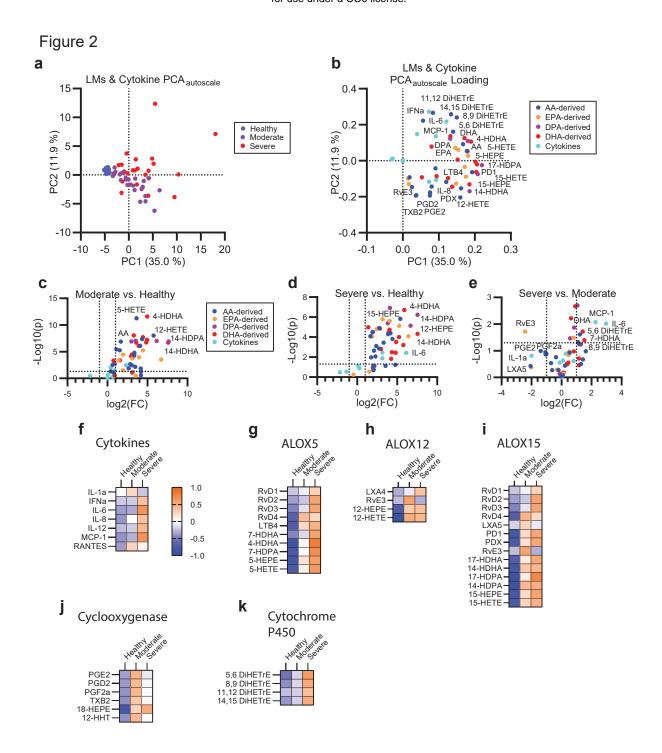|	Healthy (n=19)	Moderate (n=18)	Severe (n=20)	p-value
Demographics				
Mean Age ± SD (Range)	42.7 ± 14.92 (21-72）	60.56 ± 14.11 (26-92)	63.6 ± 15.17 (32-91）	<0.001
Mean BMI ± SD (Range)		29.65 ± 8.37 (19.49-55.04)	31.08 ± 5.84 (22.87-44)	0.5402
Gender, n (%)				0.6391
Male	9 (47.37%)	11 (61.11%)	12 (60%)	
Female	10 (52.63%)	7 (38.89%)	8 (40%)	
Race, n (%)				0.8932
White	15 (78.95%）	13 (72.22%)	14 (70%)	
Black	2 (10.53%）	2 (11.11%)	3 (15%)	
Hispanic	1 (5.26%）	2 (11.11%)	3 (15%)	
Asian	1 (5.26%）	1 (5.56%)	0 (0%)	
Comorbidities				
Heart disease		5 (27.78%)	10 (50%)	0.1983
Hyperlipidemia		4 (22.22%)	6 (30%)	0.719
Hypertension		10 (55.56%)	15 (75%)	0.3071
Chronic lung diseases		1 (5.56%)	4 (20%)	0.3436
Diabetes		5 (27.78%)	7 (35%)	0.7342
Therapies				
Tociluzimab		9 (50%)	18 (90%)	0.0113
Hydroxycloroquine		13 (72.22%)	20 (100%)	0.0171
Steroids		2 (11.11%)	8 (40%)	0.0673
Antiviral				0.5292
Azatanavir		11 (61.11%)	13 (65%)	
Remdesivir trial		2 (11.11%)	4 (20%)	
Mechanical ventilation		0 (0%)	13 (65%)	<0.0001
Intensive Care Unit		0 (0%)	20 (100%)	<0.0001

410

Figure 1

Figure 2

Figure 3